
WHAT CAN WE LEARN FROM GRADIENTS?

Jia Qian, Lars kai Hansen

Department of Applied Mathematics and Computer Science,
Technical University of Denmark,
2800 Lyngby, Denmark.
{jiaq,lkai}@dtu.dk

October 31, 2021

ABSTRACT

Recent work ([1]) has shown that it is possible to reconstruct the input (image) from the gradient of a neural network. In this paper, our aim is to better understand the limits to reconstruction and to speed up image reconstruction by imposing prior image information and improved initialization. Firstly, we show that for the **non-linear** neural network, gradient-based reconstruction approximates to solving a high-dimension **linear** equations for both fully-connected neural network and convolutional neural network. Exploring the theoretical limits of input reconstruction, we show that a fully-connected neural network with a **one** hidden node is enough to reconstruct a **single** input image, regardless of the number of nodes in the output layer. Then we generalize this result to a gradient averaged over mini-batches of size B . In this case, the full mini-batch can be reconstructed in a fully-connected network if the number of hidden units exceeds B . For a convolutional neural network, the required number of filters in the first convolutional layer again is decided by the batch size B , however, in this case, input width d and the width after filter d' also play the role $h = (\frac{d}{d'})^2 BC$, where C is channel number of input. Finally, we validate and underpin our theoretical analysis on bio-medical data (fMRI, ECG signals, and cell images) and on benchmark data (MNIST, CIFAR100, and face images).

1 Motivation

Privacy and security are major concerns in Federated Learning (FL, [2]), e.g., the member participation attack [3] revealing the presence of certain data. An important general defence is differential privacy [4]. For a relaxed differential privacy mechanism, (ϵ, δ) , the information leakage is quantified as $\exp(\epsilon)$ under the bounded leakage probability δ . Another category consists of adversarial attacks that attempt to prevent a model from being learned at all [5, 6, 7]. Typically, the attacker employs an additive GAN model to learn a generative model with the gradient updates collected from the distributed devices, even if the attacker has no access to input data.

Recent work [1] showed that an attacker may reconstruct the training data in the FL environment. In particular, the attacker does not require much auxiliary information; basically they can pretend to be an honest server or participant (with only knowledge of the gradient update and the model parameters).

Investigating the limits to this highly interesting demonstration we propose to invoke image prior information and a new initialization mechanism the primary aim is to speed up the convergence rate of reconstruction, while the secondary aim is to also increase the numerical stability. Moreover, we offer a theoretical analysis of the limitations of the reconstruction for a fully-connected neural network and vanilla convolutional neural network. Our main contributions are:

- Firstly, we unveil gradient-based reconstruction attack approximating to solve the linear equations.
- We introduce prior image knowledge and a new initialization to increase the convergence rate and successful reconstruction.

Algorithm 1 Average Federated Learning

```

1: Initialization:  $w^0$ 
2: for  $t=1,\dots,T$  do
3:    $\Rightarrow$  devices:
4:   for  $j=1,2,\dots,p$  do  $p$  devices (in Parallel)
5:      $v_j^t = \nabla \hat{\ell}_j(f(\{x_{jk}^t\}, w^t), \{y_{jk}^t\})$ 
6:     with  $(\{x_{jk}^t\}_{k=1,\dots,K}, \{y_{jk}^t\}_{k=1,\dots,K}) \sim \hat{\mathcal{D}}$ 
7:     share  $v_j^t$  with server
8:   end
9:    $\Rightarrow$  server:
10:   $w^{t+1} = w^t - \eta \times \frac{1}{p} \sum_{j=1}^p v_j^t$ 
11:  share  $w^{t+1}$  with devices for next round
12: end
13: end

```

- We show that a fully-connected neural network only needs **a single** node in **one** hidden layer to reconstruct a single input image, regardless of the number of nodes in the output layer, as long as the output layer has bias term. We generalize the result to mini-batch reconstruction and show that **the number of hidden units has to exceed the size of the mini-batch**.
- For a convolutional neural network, the number of filters in the first convolutional layer decides whether reconstruction is possible, namely, the number of filters should be such that size of output after passing through the first convolutional layer exceeds the size of original input.

2 Federated Learning

In the FL setup, we have a server and a collection of distributed devices jointly training a global model with the knowledge of the combined environment. The collection of devices own their local data, and based on which, update the gradients with the server. Thus, the global empirical loss function $\hat{\ell}(\cdot)$ can be approximated by average of local loss functions $\hat{\ell}_i$, shown in equation (1). Note that here we consider the data is independent and identically distributed across all the devices, which is not necessary for practice. We define $m = \sum_{i=1}^p m_i$ where m_i is the amount of data on device i .

$$\begin{aligned}
\hat{\ell}(X) &= \sum_{i=1}^p \frac{m_i}{m} \mathbb{E}_{(x,y) \sim D} [\hat{\ell}_i(f_w(x), y)] \\
&= \frac{1}{p} \sum_{i=1}^p \mathbb{E}_{(x,y) \sim D} [\hat{\ell}_i(f_w(x), y)] (m_i = m_j, \forall i, j)
\end{aligned} \tag{1}$$

Each iteration consists in two stages: local training and aggregation. More specifically, after distributed devices have completed local training, they share the corresponding gradients with the server, and the server aggregates the gradients based on the given criterion, updates the global model, and finally it sends the updated global model back to the devices. The devices will use this model for the next iteration. The procedure is depicted in Algorithm 1. We assume that we have p active devices participating in every round, and all the devices share the same batch size K , which induces the so-called Average Federated Learning (average gradients update, Line 10 in Algorithm 1). Data of all devices is assumed to be generated by the same underlying data distribution \mathcal{D} , denoted the empirical distribution $\hat{\mathcal{D}}$.

3 Related Work

In the FL setting, a generative adversarial network (GAN)-based attack has been proposed as a means to adversely train the global model. [8] employs a multi-task GAN whose discriminator is trained by the gradient update from the victim, interestingly with no direct access to the data. Its discriminator simultaneously discriminates for multiple tasks: category, reality, and client identity of input samples. [9] shows that it is possible to have the membership

attack and also infer properties that hold only for a subset of the training data. Another work [7] assumes that one participant is an attacker, who owns a discriminator with the same architecture as the classifier. Moreover, the attacker generates the fake images and adversely update the global model to force the victim to reveal more information. All Gan-based attacks are notorious for increasing the complexity of training the model and partially disclosing the data distribution. Most of the attacks mentioned beforehand are white-box attacks, in which attackers have access to the complete model description. For black-box attack, the attackers typically ask for the prediction or query. For instance, in one work [10], the attacker uses black-box access to the model to infer a sensitive feature x_i . More precisely, given joint distribution and marginal priors they employ maximum a posterior (MAP) estimator that may sample a promising x_i that maximizes the posterior probability. The current state-of-the-art of reconstruction is [1], their reconstruction is more accurate than the GAN-based attacks. [11] and [12] are extensions, and aim to improve the label prediction accuracy and the reconstruction loss function.

4 Reconstruction Method and Theoretical analysis

In this section, we will first introduce the reconstruction method and then offer theoretical analysis of reconstruction based on the fully-connected neural network and convolutional neural network.

4.1 Reconstruction Method

The reconstruction method is essentially an function-inversion operator, without the loss of generality, say we have any function G parameterized by w , and input $x \in \mathbb{R}^d$, which maps from x to a gradient vector v ($|v| = p$), $G : \mathbb{R}^{B \times d} \mapsto \mathbb{R}^p$ ($B = 1$, if SGD). For mini-batch, the output of the gradient function is the average gradient $\bar{v} = \frac{1}{B} \sum_{i=1}^B G(x_i, y_i; w)$. We aim to compute x with the knowledge of model parameters w and output v . If G^{-1} exists, then we have the analytical form, which is typically not the case. In FL setup, the malicious server is aware of the gradients v , model parameters w and gradient function G .

An intriguing question is that is it possible to reconstruct x in the non-reversible case? We show in Section 4.2 that one-instance reconstruction based on fully-connected neural network has the analytical form, thus can be computed directly. While, for multiple-instance reconstruction and CNN, there is no analytical form of the inverse gradient function. We convert it to the optimization problem, more specifically, we start from a random guess \hat{x} , and gradually pull it to close to the original input x by minimizing the cost function, like [1] proposed. However, we define a different cost function that includes an additive regularizer to facilitate the optimization step, as $L(\cdot) + \lambda R(\cdot)$, where $L(\cdot)$ is the distance between ground-truth gradient v and $\hat{v} = G(\hat{x}, w)$. For single instance reconstruction, we employ L2 regularizer $\lambda \|\hat{x}\|_F^2$, and for mini-batch reconstruction, we suggest an orthogonality regularizer $R = \lambda \sum_{k \neq k'=1}^n (\hat{x}_k^\top \hat{x}_{k'})^2$, and keep λ decay over the iterations. The pseudo code is described in Algorithm 2.

Our method is numerically more stable by two modifications relative to [1]. First, we sample the dummy (initial) data from an uniform distribution on the interval $x \sim \mathbb{U}(0, 1)$ since typically the preprocessing operation re-scale image data into the range between zero and one. Second, we expand the cost function with an orthogonal regularizer $\lambda \sum_{k \neq k'=1}^n (\hat{x}_k^\top \hat{x}_{k'})^2$ for mini-batch reconstruction. It leads to three following advantages: 1) Due to the appropriate initialization, it starts from a promising position (in the solution space) close to the optima x^* . 2) For the single instance reconstruction, L2 as our regularizer forces $\|\hat{x}\|_F^2$ small (in particular in the early stage of iterations), which may avoid the gradient saturation for activation function like sigmoid and also prevent it from going too far from the possible zone $([0, 1])$ during the iterative optimization, increasing numerical stability. 3) For the mini-batch reconstruction, the orthogonal regularizer may penalize the similarities between reconstructed images, in particular, in the early optimization stage.

4.2 Reconstruction of Fully-connected Neural Network

Proposition 1 (INVERSE OF SIGMOID FUNCTION). *Given the value $y = \sigma(x)$, then we have the unique corresponding value $\sigma'(x) = \sigma(\frac{y}{1-y})(1 - \sigma(\frac{y}{1-y}))$.*

Proof. We know $\sigma(x) = \frac{1}{1+e^{-x}} = y$, thus we have $x = \log(\frac{y}{1-y})$. And the derivative of sigmoid function w.r.t x is $\frac{\partial}{\partial x} \sigma(x) = \frac{\partial}{\partial x} [\frac{1}{1+e^{-x}}] = \sigma(x) \cdot (1 - \sigma(x))$, so $\sigma'(x) = \sigma(\frac{y}{1-y})(1 - \sigma(\frac{y}{1-y}))$. \square

Say we have a one-layer fully-connected neural network f , with n_1 units in hidden layer and n_2 units in output layer (if classification task, n_2 is equal to number of classes). Thus, we can define $a_j = f_w(x) = w_{ji}^2 \sum_{i=1}^{n_1} \sigma(w_i^1 x + b_i^1) + b_j^2$,

Algorithm 2 *Our Reconstruction (with improved initialization and regularizer)*

```

1: Input:  $v, w$ 
2: for  $i=0,1,2,\dots,I$  do  $I$  iterations
3:   if  $i==0$  then
4:      $\hat{x}_0, \hat{y}_0 \sim \mathcal{U}(\mathbb{0}, \mathbb{1})$ 
5:      $\hat{v}_1 = G(\hat{x}_0, \hat{y}_0; w)$ 
6:   else
7:      $\hat{v}_i = G(\hat{x}_i, \hat{y}_i; w)$ 
8:     if single reconstruction then
9:        $\min_{\hat{x}_i, \hat{y}_i} \|v - G(\hat{x}_i, \hat{y}_i; w)\|_2^2 + \lambda \|\hat{x}_i\|_F$ 
10:    else
11:       $\min_{\hat{x}_i, \hat{y}_i} \|v - G(\hat{x}_i, \hat{y}_i; w)\|_2^2 + \lambda \sum_{k \neq k'=1}^n (\hat{x}_k^\top \hat{x}_{k'})^2$ 
12:    end
13:    update:  $\hat{x}_{i+1} = \hat{x}_i - \eta \times \nabla L_{\hat{x}_i}$ 
14:     $\hat{y}_{i+1} = \hat{y}_i - \eta \times \nabla L_{\hat{y}_i}$ 
15:  if  $(i/m)==0$  then
16:     $\lambda = 0.9 * \lambda$ 
17:  end
18: end

```

where w^1 and b^1 are the weights and bias in hidden layer, and w^2 , b^2 in output layer and $\sigma(x) = \frac{1}{1+e^{-x}}$ is the monotonic activation function sigmoid. For the classification task, we employ cross-entropy as the cost function $\ell(p_i, y_i) = -\sum_j^C y_{ij} \log p_{ij}$ where p_i is a vector with length equal to the number of classes C , and $p_{ij} = \frac{e^{a_j}}{\sum_k e^{a_k}}$ after softmax function.

Proposition 2 (FULLY-CONNECTED NEURAL NETWORK ONE-INSTANCE RECONSTRUCTION). *To reconstruct one input based on a fully-connected neural network, we have the analytical form to compute the lossless input, with only **single** unit in the hidden layer regardless of the number of nodes in **one** output layer, as long as bias term exists.*

$$\frac{\partial \ell}{\partial a_j} = -\sum_k y_k \frac{\partial \log p_k}{\partial a_j} = -\sum_k y_k \frac{1}{p_k} \frac{\partial p_k}{\partial a_j} \quad (2)$$

$$\frac{\partial p_i}{\partial a_j} = \begin{cases} p_j(1-p_j), & i = j \\ -p_j p_i, & i \neq j \end{cases} \quad (3)$$

$$\begin{aligned} \frac{\partial \ell}{\partial a_j} &= -\left[\frac{y_j}{p_j}(p_j(1-p_j)) - \sum_{k \neq j} \frac{y_k}{p_k} p_j p_k\right] \\ &= -y_j(1-p_j) + \sum_{k \neq j} (y_k p_j) \\ &= p_j - y_j \end{aligned} \quad (4)$$

Plug eq. (3) into eq. (2), we have eq. (4). Thus, all the partial derivatives are as the followings:

$$\frac{\partial \ell}{\partial b_j^2} = p_{.j} - y_{.j} \quad (5)$$

$$\frac{\partial \ell}{\partial w_{ji}^2} = (p_{.j} - y_{.j}) \sigma(w_i^1 x + b_i^1) = (p_{.j} - y_{.j}) \sigma_i \quad (6)$$

$$\frac{\partial \ell}{\partial b_j^1} = \sum_i^{n_2} (p_{.i} - y_{.i}) w_{ij}^2 \sigma'(w_j^1 x + b_j^1) = \sum_i^{n_2} (p_{.i} - y_{.i}) w_{ij}^2 \sigma'_j \quad (7)$$

$$\frac{\partial \ell}{\partial w_j^1} = \sum_i^{n_2} (p_{.i} - y_{.i}) w_{ij}^2 \sigma'_j x \quad (8)$$

For the one-instance reconstruction where $x \in \mathbb{R}^d$, from eq. (8), we can directly compute $x_i = \frac{\partial \ell}{\partial w_{1i}^1} / \frac{\partial \ell}{\partial b_1^1}, \forall i \in [1, d]$. For the non-linear neural network, the single instance reconstruction is actually have the simple analytical form. It can be generalized to multiple-hidden-layer fully-connected neural network (last layer is L). The partial derivative w.r.t the bias term in the first hidden layer is $\frac{\partial \ell}{\partial b_n^1} = \sum_{h=1}^{n_L} (p_{.h} - y_{.h}) \sum_{j=1}^{L-1} w_{hj}^L (\sigma_j^{L-1})' w_{ji}^{L-1} \dots w_{mn}^2 (\sigma_n^1)'$. And the partial derivative w.r.t weights in the first hidden layer is $\frac{\partial \ell}{\partial w_n^1} = \sum_{h=1}^{n_L} (p_{.h} - y_{.h}) \sum_{j=1}^{L-1} w_{hj}^L (\sigma_j^{L-1})' w_{ji}^{L-1} \dots w_{mn}^2 (\sigma_n^1)' x$.

It is far more complicated for mini-batch reconstruction since we typically know the average gradient or the sum of gradient and aim to reconstruct individual instance. we refer this procedure as *demixing* in the following context.

Proposition 3 (FULLY-CONNECTED NEURAL NETWORK MINI-BATCH RECONSTRUCTION). *For the mini-batch reconstruction, with the assumption that given sigmoid $\sigma(x)$, we may compute the unique $\sigma'(x)$, we derive the condition that the number of units in hidden layer $n_1 \geq \frac{B(d+n_2)-n_2}{d+n_2+1-B}$. For the high-dimensional input, whose dimension $d \gg n_2, d \gg B$, n_1 is dominated by $\frac{B(d+n_2)}{d+n_2}$, thus $n_1 \geq B$.*

For instance, if we have a mini-batch of size two, then we have $\frac{\partial \ell}{\partial w_i^1} = [(f_{11} - t_{11})w_{1i}^2 + (f_{12} - t_{12})w_{2i}^2]\sigma'_{i1}x_1 + [(f_{21} - t_{21})w_{1i}^2 + (f_{22} - t_{22})w_{2i}^2]\sigma'_{i2}x_2$. w^2 is known from model parameters, assuming that $(f_{ij} - t_{ij}), \sigma'_{ij}$ are also known, then we can rewrite it as $c_1x_1 + c_2x_2 = b$. From **proposition 1**, we can compute σ'_{ij} known σ_{ij} . In this case, x_1 and x_2 are mixed together in the equation, which can be solved by Gaussian elimination. Moreover, the left hand of this equation will increase the complexity with the batch size increment $\sum_{m=1}^n c_mx_m = b$. Theoretically, if the number of equations is identical or greater than batch size and all the equations are independent, it is solvable. However, practically it is not easy to solve, and we normally solve it by converting it to the optimization problem. The acute readers might notice that the order of instances doesn't matter, which means it has $B!$ solution, where B is the batch size. Besides, the updated input value during optimization might introduce the saturation of sigmoid function ($\sigma(x) \approx 0, \sigma(x) \approx 1$ regardless the change of x outside $[-4, 4]$). Finally, the high-dimension input x also increases the difficulty of solving the optimization problem. The choice of optimization method is relatively sensitive. For a high-dimension (nonsparse) input, second-order or quasi-second-order methods sometimes fails since it is designed to search for the zero-gradient position. The number of saddle points exponentially increases with the number of input dimensions [13]. First-order method, e.g., Adam takes much more iterations to converge, but it is relatively more stable, likely to escape from the saddle points [14]. Please see the appendix A.1, we offer the complete derive of a tiny sample.

4.3 Reconstruction of Convolutional Neural Network

For a single-convolutional layer CNN (no pooling), the kernel parameters (kernel size, padding size, stride s) determine the output size after convolutional layers. More specifically, say we have input $x \in \mathbb{R}^{C*d*d}$, for the simplicity we assume height and width are identical. After convolutional layer, the width of output is $d' = \frac{d+2p-k}{s} + 1$, where p is padding size, k is kernel size, and s is stride size.

Proposition 4 (SINGLE LAYER CONVOLUTIONAL NEURAL NETWORK RECONSTRUCTION). *For a single-convolutional-layer neural network (without pooling) with kernel size k , padding size p and stride size s , immediately stacked by a fully-connected layer, known with n_2 units. To reconstruct, $h = (\frac{d^2}{d'})^2 BC$ filters are required, where C is the channel number of input, B is batch size, d is the width of input, and d' is width after passing one filter.*

Say we have input x with both width and length equal to d , $x \in \mathbb{R}^{B*C*d*d}$, where C is the channels and B is mini-batch size. After padding, it is labeled as \hat{x} , and its width is equal to $d + 2p$ with padding size p . We define a square kernel with width k , stride size s , bias term b , and we have h kernels. We define the output of convolutional layer shown in eq. (9), and more specifically the convolutional operator can be defined in eq. 10 (before vectorization operation).

$$z_{\underline{m}} = \sum_{c=1}^C x_c \otimes w_{\underline{m}c}^1 + b_{\underline{m}}^1 \quad (9)$$

$$z_{\underline{m}ij} = \left(\sum_{c=1}^C \sum_{g=1}^k \sum_{n=1}^k w_{\underline{m}cgh}^1 \hat{x}_{c,si+g-1,sj+n-1} \right) + b_{\underline{m}}^1 \quad \forall (i, j) \in [1, d'] \times [1, d'], \forall \underline{m} \in [1, h] \quad (10)$$

The we define $H = [\text{vec}(z_{1..}), \text{vec}(z_{2..}), \dots, \text{vec}(z_{h..})]$ and $|H| = h(d')^2 = n_1$, after convolutional layer we have $p_j = \sum_{i=1}^{n_1} w_{ji}^2 \sigma(H_i) + b_j^2$, where $w^2 \in \mathbb{R}^{n_2*n_1}$ and $b^2 \in \mathbb{R}^{n_2}$ are the weights and bias in the output layer, $\sigma(\cdot)$ is the

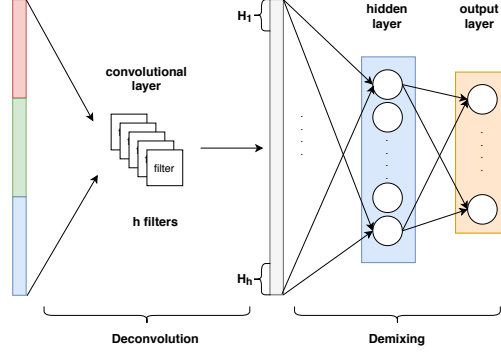


Figure 1: For a single-convolutional layer neural network (no pooling), to fully reconstruct input, we need h filters such that size of the filtered output (grey rectangle) stays close to the size of original input (red, green and blue parts).

sigmoid function as defined before. Thus,

$$\frac{\partial \ell}{\partial b_j^2} = p_{.j} - y_{.j} \quad \forall j \in [1, n_2] \quad (11)$$

$$\frac{\partial \ell}{\partial w_{ji}^2} = (p_{.j} - y_{.j})\sigma(H_i) \quad \forall j \in [1, n_2], \forall i \in [1, n_1] \quad (12)$$

$$\frac{\partial \ell}{\partial b_{\underline{m}}^1} = \sum_{i=1}^{d'} \sum_{j=1}^{d'} \frac{\partial \ell}{\partial z_{mij}} \frac{\partial z_{mij}}{\partial b_{\underline{m}}^1} = \sum_{i=1}^{d'} \sum_{j=1}^{d'} \frac{\partial \ell}{\partial z_{mij}} \quad \forall \underline{m} \in [1, h] \quad (13)$$

$$\frac{\partial \ell}{\partial w_{mcgh}^1} = \sum_{i=1}^{d'} \sum_{j=1}^{d'} \frac{\partial \ell}{\partial z_{mij}} \hat{x}_{c, si+g-1, sj+h-1} \quad \forall \underline{m} \in [1, h] \quad (14)$$

Note here, $\frac{\partial \ell}{\partial z_{mij}} = \frac{\partial \ell}{\partial H[(m-1)*(d')^2+(i-1)*d'+j]}$. For the theoretically lossless reconstruction, the number of equations should meet the number of unknowns. From eq. (10), we have $(d')^2 h$ equations and $d^2 BC$ unknowns, thus we need $h = (\frac{d^2}{d'})^2 BC$, with the assumption that H is known (left hand side of eq. (10)). As shown in eq. (11) and (12), if $n_1 \geq \frac{n_2(B-1)}{n_2-B}$, and $1 < B < n_2$, all $\sigma(H_i)$ are known, thus H_i are also known since $\sigma(\cdot)$ is monotonic activation function.

Generally speaking, CNN reconstruction can be seen as a two-stage reconstruction (shown in Figure 1): *demixing* and *deconvolution*. Namely, the demixing stage is essentially a fully-connected neural network reconstruction, and we aim to reconstruct the output of convolutional layer (a.k.a the input of fully-connected layer). The deconvolution stage we want to reverse the convolutional step, starting from the output of convolutional layer to reconstruct the original input. For the demixing stage, we can borrow the idea from fully-connected neural network, as long as the number of hidden units is equal or greater than the batch size, then theoretically we may evaluate the individual instance.

Generalizing it to the multiple-convolutional-layer neural network, the output H^{i-1} of layer $i-1$ is the input of layer i , then we can express it as the following, where h^{i-1} is the number of filters in layer $i-1$ and k^{i-1} is the kernel width in layer $i-1$.

$$H_{mij}^i = \left(\sum_{c=1}^{h^{i-1}} \sum_{g=1}^{k^{i-1}} \sum_{n=1}^{k^{i-1}} w_{mcgn}^i H_{c, si+g-1, sj+n-1}^{i-1} \right) + b_m^i \quad (15)$$

5 Experimental Results

5.1 Dataset

ECG signal is derived from the MIT-BIH Arrhythmia Dataset and PTB Diagnostic ECG Database. It has been normalized to the same length 187, totally has 87554 segments. FMRI is the brain tumor dataset containing 3064 images from 233 patients with three kinds of brain tumor (meningioma, glioma, pituitary), available here. The Malaria cell images

are produced from the thin blood smear slide images, with size $3 * 32 * 32$, available here. Mnist is the handwritten digits, with size $1 * 32 * 32$ and totally 10 classes, and cifar100 has size $3 * 32 * 32$, totally with 100 classes.

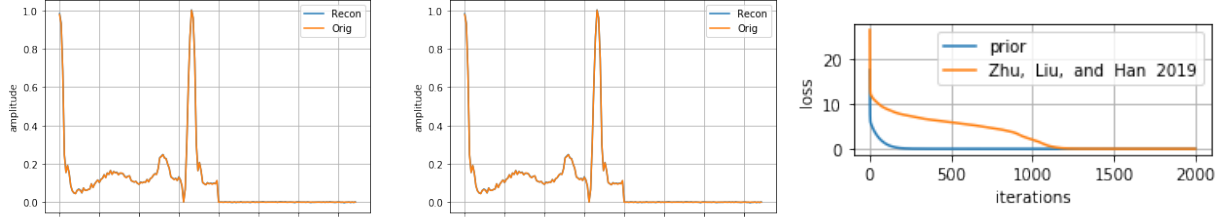


Figure 2: *ECG*: Leftmost one is final reconstruction by our method, whereas the middle one is produced by [1]. Rightmost plot shows that our method converges much faster than [1].

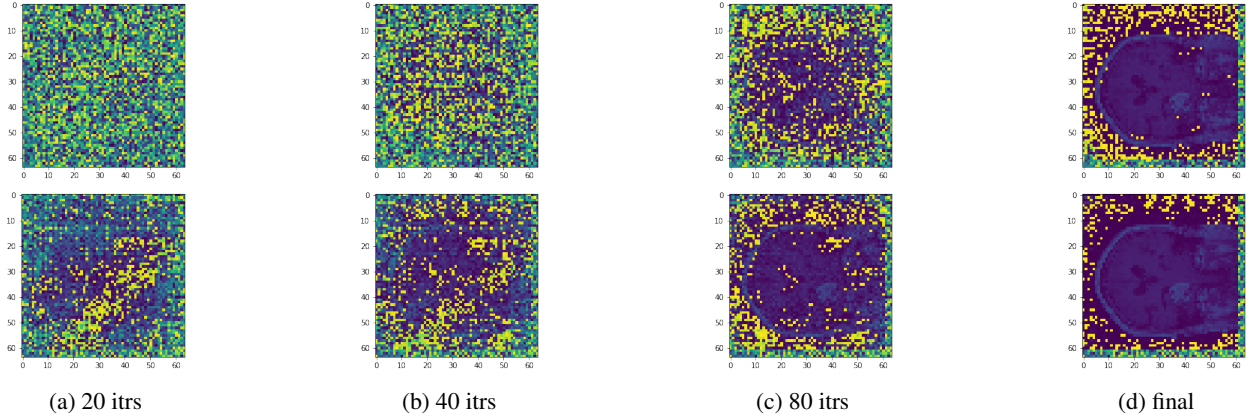


Figure 3: *FMRI*: The plots (first row) are produced by [1], and it shows the reconstructions after 20, 40, 80, and final iteration accordingly, whereas the second row is our reconstruction.

5.2 Comparison with baseline

Our reconstruction enables a faster convergence rate and a more stable reconstruction procedure comparing with the method proposed by [1]. We demonstrate the superiority of our method on ecg dataset, face dataset, fmri dataset, cell dataset, and cifar100 dataset in Figure 2, 3, 4, 13(appendix) and 14(appendix). We plot the single-instance reconstruction with the optimizer LGBFS the same as [1] did for the fair comparison, and it clearly shows that our method converges faster on all the dataset. Moreover, due to the improved initialization and regularizer, sometimes our reconstruction turns out the lower error than [1], one instance is shown in Figure 13(appendix).

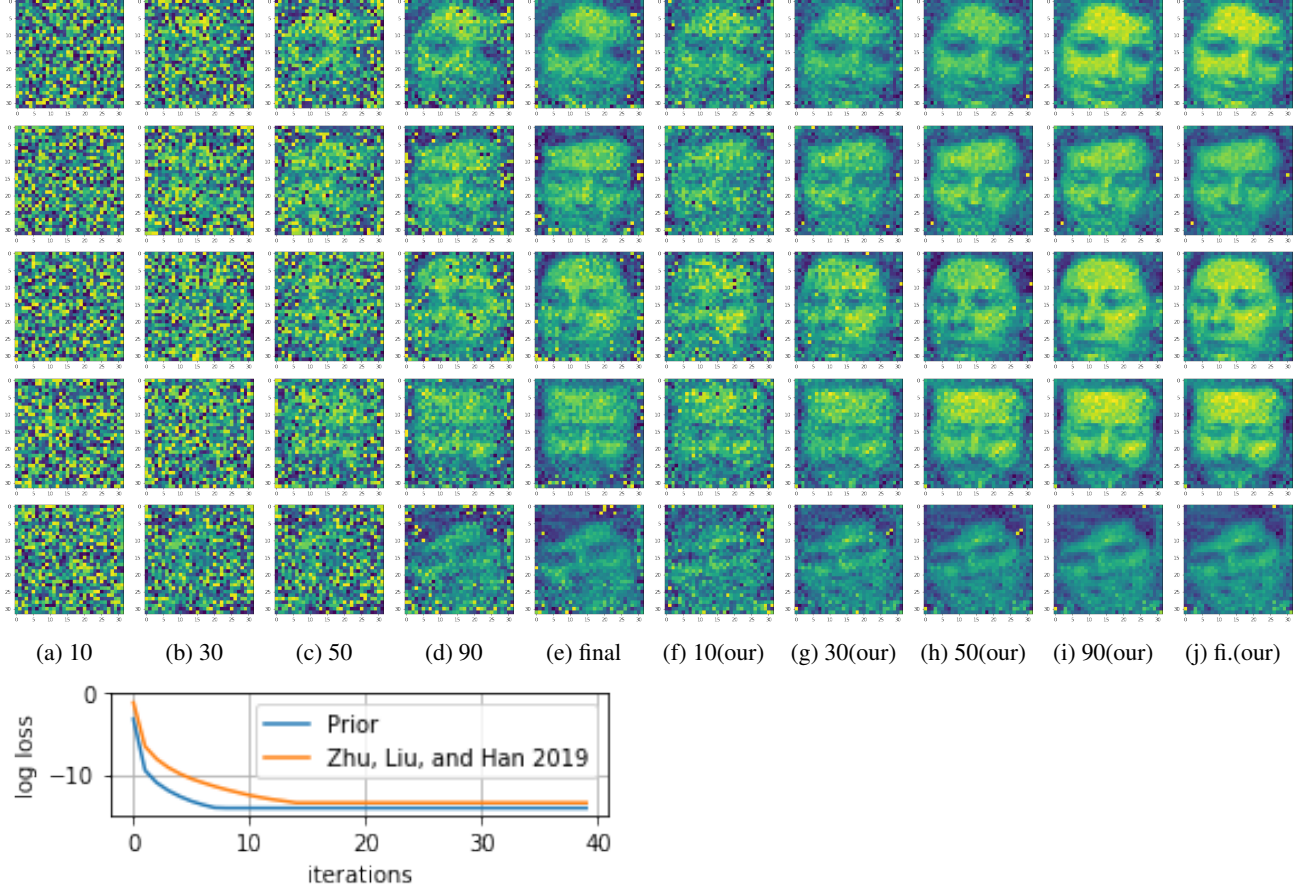


Figure 4: *Face* (Batch reconstruction): Mini-batch contains 5 images, and we show partial reconstruction for 10 (col.1), 30 (col.2), 50(col.3), 90 (col.4) and final (col.5) iteration for [1]. The rest columns (f-j) are produced by our method. Only three instances are shown due to the length limitations.

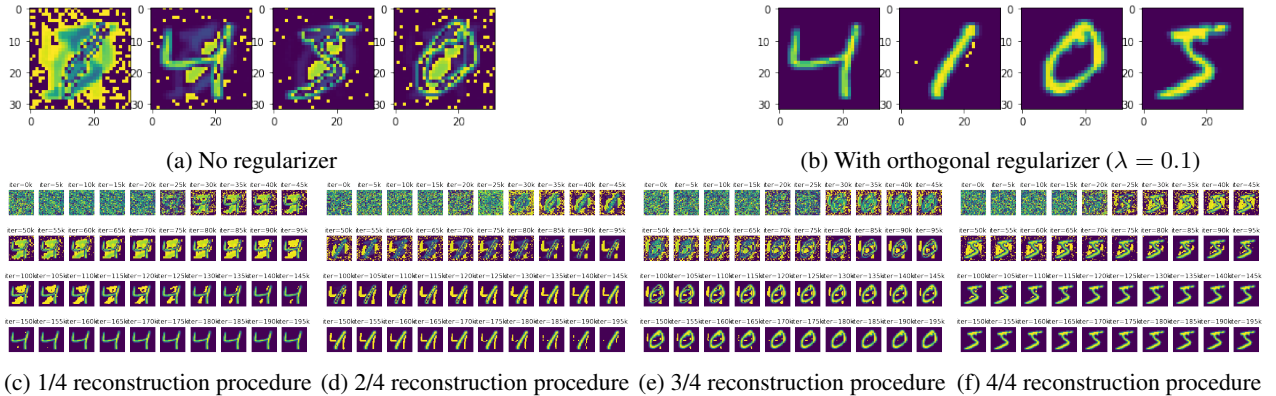
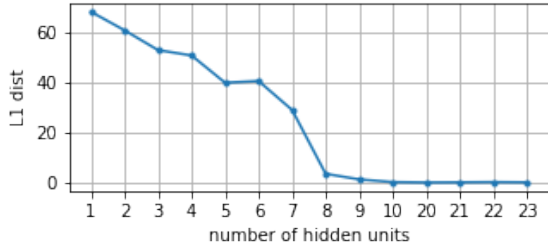


Figure 5: *MNIST* (Batch reconstruction): 5a shows the final reconstruction without any regularizer; as a comparison, with regularizer is shown in 5b. Moreover, the full reconstructions of 5b are shown in 5c, 5d, 5e and 5f. We plot every 5k iterations.

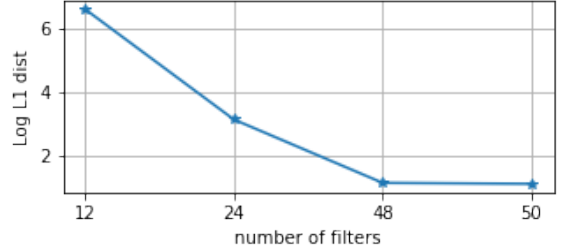
5.3 Mini-batch reconstruction

Fully-connected neural network batch reconstruction: We experiment on mnist (size: 1024) to validate our analysis; as long as the number of nodes in the hidden layer exceeds batch size, we may have the reconstruction given

sufficient iterations. Here we set batch size equal to four and number of units in hidden layer to four as well. In Figure 5a, we first give the final reconstruction of four inputs without regularizer, the digits overlap together. In Figure 5b, the performance with orthogonal regularizer improves significantly. Furthermore, from Figure 5c to 5f, we show the whole reconstruction procedure every 5k iterations, and we can see how the orthogonal regularizer plays the key role during optimization procedure to hinder the similarities between instances. Empirically, it shows that high-dimension demixing is very challenging and the the existence of orthogonality regularizer decides whether the reconstruction is successful. Moreover, in Figure 6a, we show a mini-batch reconstruction with batch size 8, however, the initialization starts from the position close to the solution (oracle initialization). Namely, we add the noise to the original input, and from which we initialize the reconstruction, only for the purpose of demonstrating the correlation between number of hidden units and batch size. It demonstrates that L1 distance between original input and reconstructed one decreases drastically with 8 units in hidden layer, afterwards even with more units, the distance does not improve too much.



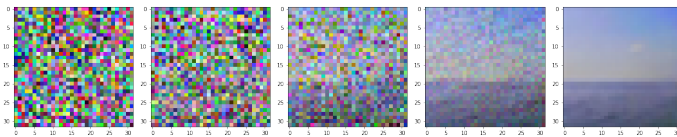
(a) MNIST reconstruction with batch size 8, when number of units in hidden layer surpass the batch size, the distance between reconstructed image and original one drastically decreases.



(b) CIFAR100 reconstruction with batch size 4, kernel size 5, padding size 2, stride size 2. According to proposition 3, 48 filters are required. Reconstruction is shown in Figure 8.

Figure 6: L1 distance and number of units and filters

Cnn batch reconstruction: We test on the cifar100 dataset, with kernel size 5, padding size 2 and stride size 2. According to **Proposition 4**, we need 12 filters to reconstruct one instance. In Figure 11, we visually show the reconstruction performance with the change of filters number and from Table 7f, we show L1 distance alters with filter number. Note here we set λ starts from 0.1 and gradually decays 90% after 2k iterations. For the mini-batch reconstruction (shown in Figure 6b), we set batch size equal to four, thus 48 filters are required, we compared filter number equal to 12, 24, 48 and 50, as we can see the L1 distance keeps decreasing and the reconstruction is in Figure 8. In particular, when filter number is 48, average L1 distance per pixel is 0.00025.



(a) 1 filter (b) 5 filters (c) 8 filters (d) 11 filters (e) 12 filters

Filters	Params. $((b')^2h)$	L1 dist.
1	64	728
5	1280	649
8	2048	404
11	2816	135
12	3072	0.57

(f) L1 distance

Figure 7: *One-layer CNN*: Image reconstruction becomes more accurate with increasing number of filters (kernels). Numerical comparison sees Table 7f. *One-layer CNN*: Distance decreases with increasing number of filters (kernels). First row is the number of filters, and second row is the size of filtered images, which is decided by the number of filters with the fixed kernel, padding and stride size. When the size of filtered image is exactly equal to original input size (12 filters), we can almost perfectly reconstruct it (L1 distance is 0.09, with λ starts from 0.1)

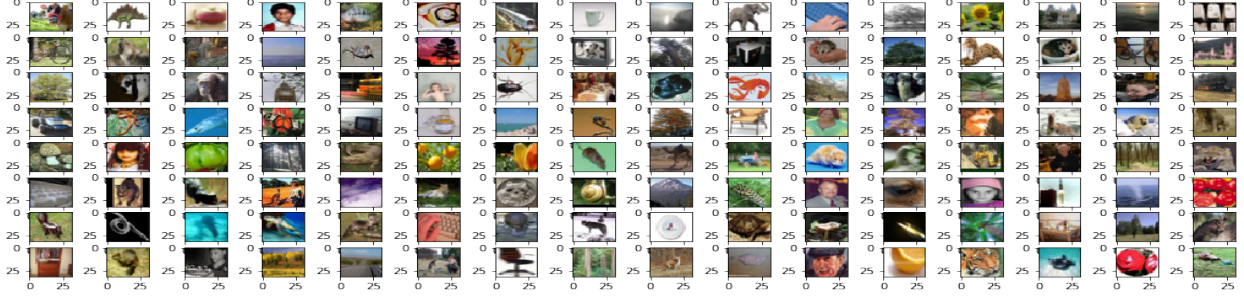


Figure 10: CNN two-stage reconstruction with batch size 128. Visually the reconstruction is almost lossless (average L1 distance (per image) with original input is 0.04), with the assumption that the demixing stage is perfectly recovered.

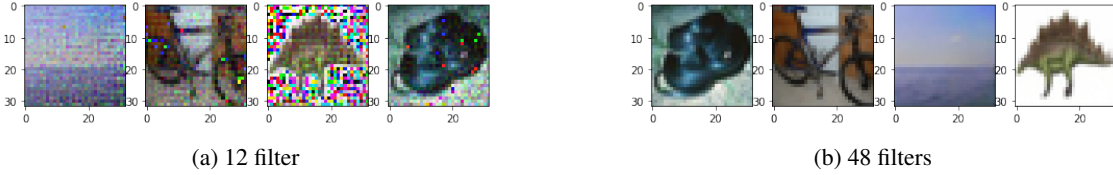


Figure 8: CIFAR100 reconstruction with batch size 4 with 12 and 48 filters. λ starts from 0.1, and gradually decays.

Batch size limitation: As we mentioned before, the batch size stays in the range $1 < B < n_2$, where n_2 is the number of units in output layer. In Figure 9, we set the experiment where a batch of three instances of different classes is to be reconstructed (based on CNN) with three, four and five nodes locating in output layer accordingly. More specifically, with three nodes, one instance fails the reconstruction completely; whereas with four nodes, all of the three instances are reconstructed to some extent; and with five nodes they are well reconstructed. Again, the number of nodes in output layer determines the success of demixing step in CNN.

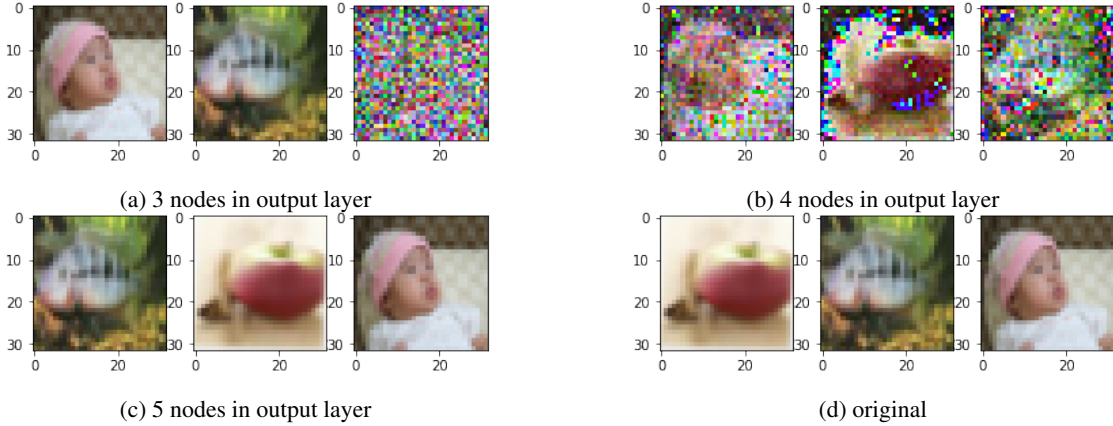


Figure 9: CIFAR100 reconstruction with batch size 3 (three instances with different classes, thus cannot conduct experiment with 2 nodes in output layer, with three, four and five nodes in output layer.)

Deconvolution: The experiment shows that deconvolution is much easier in terms of reconstruction. In Figure 10, we show that a batch with 128 images can be well reconstructed if the demixing step is solved, even with the permuted order of the demixing output (output after convolutional layer).

Generalized CNN: Finally, we extend the conclusion of required filters to a two-layer CNN, according to **Proposition 4**, 12 filters are required for a single-layer CNN and 48 filters are for a two-layer CNN. The experimental results shown in Figure 11, 12 validate our conclusions.

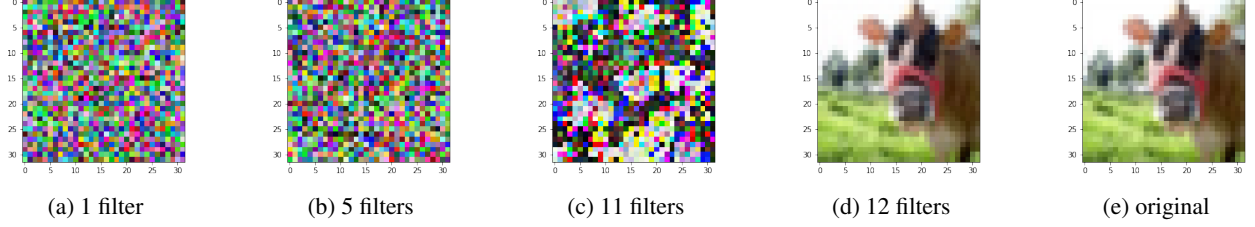


Figure 11: *One-layer CNN*: (First row) we show that the image reconstruction becomes more accurate with increasing number of filters (kernels), moreover, when filter number is equal to 12, reconstructed input is almost the same as the original input (with bare eyes). (Second row) we plot the L1 distance between reconstructed input and original one.

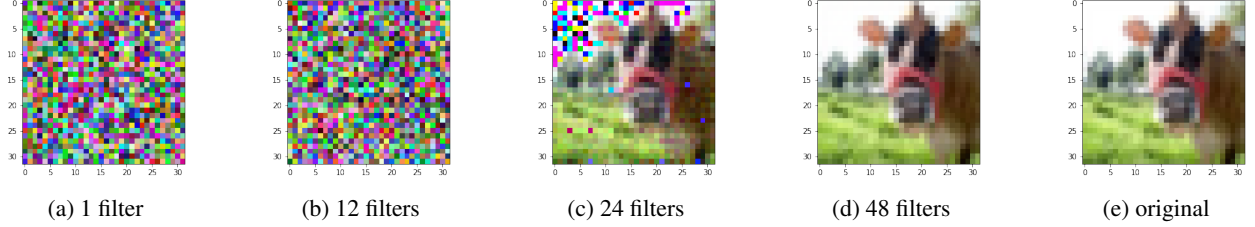


Figure 12: *Two-layer CNN*: We separately show the reconstruction for different numbers of filters on the second convolutional layer. Note here 12 filters are sitting in the first layer.

6 Conclusion

We have investigated the highly interesting results in [1] to understand if the results can be improved by careful initialization and augmenting the cost function with regularizers. More specifically, we suggest an uniform distribution $([0,1])$ initialization since typically the preprocessing re-scales it between zero and one. We propose a L2 regularizer for single image reconstruction, and an orthogonality promoting regularizer for mini-batch reconstruction. In both cases we let the strength λ decay during iterations, to reduce bias in the final solutions. Then, we explore the limitation of reconstruction and analyze the correlation between architecture, network size, and reconstruction performance. We show that a fully-connected neural network only needs a single node in one hidden layer to reconstruct a single input image, regardless of the number of nodes in the output layer, as long as bias term exists. For the mini-batch case, as long as the number of nodes in the first hidden layer exceeds the batch size (with regularizer), the reconstruction is promising. For the convolutional neural network, $(\frac{d}{d'})^2 C$ filters are required for the reconstruction, where d is the width of input image, d' is the width after one convolutional filter, and C is input channel number. It can be generalized to mini-batch reconstruction as well, thus $BC * (\frac{d}{d'})^2$ filters are required (B is batch size).

A Appendix

A.1 Fully-connected neural network

Say we have n_1, n_2 nodes in hidden and output layer accordingly, and batch size is B . A one-hidden-layer neural network is defined as $p_j = \sum_{i=1}^{n_1} w_{ji}^2 \sigma(w_i^1 x + b_i^1) + b_j^2$, where $\sigma()$ is a monotonic active function, and σ_{ij} indicates $\sigma(w_i x_j + b_i)$ in the current layer, and j is the index for instance x_j . Our cost function E is cross entropy.

$$\frac{\partial \ell}{\partial b_j^2} = f_{.j} - t_{.j} \quad (16)$$

$$\frac{\partial \ell}{\partial w_{ji}^2} = (f_{.j} - t_{.j}) \sigma(w_i^1 x + b_i^1) = (f_{.j} - t_{.j}) \sigma_i \quad (17)$$

$$\frac{\partial \ell}{\partial b_i^1} = \sum_j^{n_2} (f_{.j} - t_{.j}) w_{ji}^2 \sigma_i' \quad (18)$$

$$\frac{\partial \ell}{\partial w_i^1} = \sum_j^{n_2} (f_{.j} - t_{.j}) w_{ji}^2 \sigma_i' x \quad (19)$$

For the purpose of demonstration, we set batch size B equal to 2, n_1 equal to 3, n_2 equal to 2.

$$\text{derive from eq. (16)} \begin{cases} \frac{\partial \ell}{\partial b_1^2} = (f_{11} - t_{11}) + (f_{21} - t_{21}) \\ \frac{\partial \ell}{\partial b_2^2} = (f_{12} - t_{12}) + (f_{22} - t_{22}) \end{cases} \quad (20)$$

$$\text{derive from eq. (17)} \begin{cases} \frac{\partial \ell}{\partial w_{11}^2} = (f_{11} - t_{11})\sigma_{11} + (f_{21} - t_{21})\sigma_{12} \\ \frac{\partial \ell}{\partial w_{12}^2} = (f_{11} - t_{11})\sigma_{21} + (f_{21} - t_{21})\sigma_{22} \\ \frac{\partial \ell}{\partial w_{13}^2} = (f_{11} - t_{11})\sigma_{31} + (f_{21} - t_{21})\sigma_{32} \\ \frac{\partial \ell}{\partial w_{21}^2} = (f_{12} - t_{12})\sigma_{11} + (f_{22} - t_{22})\sigma_{12} \\ \frac{\partial \ell}{\partial w_{22}^2} = (f_{12} - t_{12})\sigma_{21} + (f_{22} - t_{22})\sigma_{22} \\ \frac{\partial \ell}{\partial w_{23}^2} = (f_{12} - t_{12})\sigma_{31} + (f_{22} - t_{22})\sigma_{32} \end{cases} \quad (21)$$

$$\text{derive from eq. (18)} \begin{cases} \frac{\partial \ell}{\partial b_1^1} = [(f_{11} - t_{11})w_{11}^2 + (f_{12} - t_{12})w_{21}^2]\sigma'_{11} + [(f_{21} - t_{21})w_{11}^2 + (f_{22} - t_{22})w_{21}^2]\sigma'_{12} \\ \frac{\partial \ell}{\partial b_2^1} = [(f_{11} - t_{11})w_{12}^2 + (f_{12} - t_{12})w_{22}^2]\sigma'_{21} + [(f_{21} - t_{21})w_{12}^2 + (f_{22} - t_{22})w_{22}^2]\sigma'_{22} \\ \frac{\partial \ell}{\partial b_3^1} = [(f_{11} - t_{11})w_{13}^2 + (f_{12} - t_{12})w_{23}^2]\sigma'_{31} + [(f_{21} - t_{21})w_{13}^2 + (f_{22} - t_{22})w_{23}^2]\sigma'_{32} \end{cases} \quad (22)$$

$$\text{derive from eq. (19)} \begin{cases} \frac{\partial \ell}{\partial w_1^1} = [(f_{11} - t_{11})w_{11}^2 + (f_{12} - t_{12})w_{21}^2]\sigma'_{11}x_1 + [(f_{21} - t_{21})w_{11}^2 + (f_{22} - t_{22})w_{21}^2]\sigma'_{12}x_2 \\ \frac{\partial \ell}{\partial w_2^1} = [(f_{11} - t_{11})w_{12}^2 + (f_{12} - t_{12})w_{22}^2]\sigma'_{21}x_1 + [(f_{21} - t_{21})w_{12}^2 + (f_{22} - t_{22})w_{22}^2]\sigma'_{22}x_2 \\ \frac{\partial \ell}{\partial w_3^1} = [(f_{11} - t_{11})w_{13}^2 + (f_{12} - t_{12})w_{23}^2]\sigma'_{31}x_1 + [(f_{21} - t_{21})w_{13}^2 + (f_{22} - t_{22})w_{23}^2]\sigma'_{32}x_2 \end{cases} \quad (23)$$

To fully solve $x_1, x_2 \in \mathbb{R}^d$, we need to meet the condition that $n_2 + n_1n_2 + n_1 + n_1d \geq Bn_2 + n_1B + Bd$, thus $n_1 \geq \frac{Bn_2+Bd-n_2}{n_2+1+d-B}$. Typically we have $d \gg n_2, d \gg B$, thus $n_1 \geq B$

A.2 Convolutional neural network

Say we have input $x \in \mathbb{R}^{B \times C \times d \times d}$ passing through one convolutional layer with h kernels and h bias, and then feeding into the fully-connected layer with n_2 units. Each filter has width k , padding size p . After padded, x has width $d + 2p$, and after one kernel x has width $d' = \frac{d-k+2p}{s} + 1$. Thus, after filter m , the output is defined as $z_{mij} = (\sum_{c=1}^C \sum_{g=1}^k \sum_{h=1}^k w_{mcgh}^1 \hat{x}_{c,si+g-1,sj+h-1}) + b_{\underline{m}}^1, \forall (i, j) \in [1, d'] \times [1, d'], \forall \underline{m} \in [1, h]$, and \hat{x} is the padded input. We rewrite $H = [\text{vec}(z_{1..}), \text{vec}(z_{2..}), \dots, \text{vec}(z_{h..})]$ and $|H| = h * d' * d' = n_1$, after convolutional layer, we have $p_j = \sum_{i=1}^{n_1} w_{ji}^2 \sigma(H_i) + b_j^2$, where $w^2 \in \mathbb{R}^{n_2 \times n_1}$ and $b^2 \in \mathbb{R}^{n_2}$ are the weights and bias in the output layer, $\sigma(\cdot)$ is the sigmoid function as defined before.

$$\frac{\partial \ell}{\partial b_j^2} = p_j - y_j \quad \forall j \in [1, n_2] \quad (24)$$

$$\frac{\partial \ell}{\partial w_{ji}^2} = (p_j - y_j)\sigma(H_i) \quad \forall j \in [1, n_2], \forall i \in [1, n_1] \quad (25)$$

$$\frac{\partial \ell}{\partial b_{\underline{m}}^1} = \sum_{i=1}^{d'} \sum_{j=1}^{d'} \frac{\partial \ell}{\partial z_{mij}} \frac{\partial z_{mij}}{\partial b_{\underline{m}}^1} = \sum_{i=1}^{d'} \sum_{j=1}^{d'} \frac{\partial \ell}{\partial z_{mij}} \quad \forall \underline{m} \in [1, h] \quad (26)$$

$$\frac{\partial \ell}{\partial w_{mcgh}^1} = \sum_{i=1}^{d'} \sum_{j=1}^{d'} \frac{\partial \ell}{\partial z_{mij}} \hat{x}_{c,si+g-1,sj+h-1} \quad \forall \underline{m} \in [1, h] \quad (27)$$

Note here, $\frac{\partial \ell}{\partial z_{mij}} = \frac{\partial \ell}{\partial H_{(m-1)*(d')^2+(i-1)*d'+j}} = \frac{\partial \ell}{\partial H_r} = \sum_{m=1}^{n_2} (p_m - y_m)w_{mr}^2\sigma'_r$. For the purpose of demonstration, we set B equal to 2, h equal to 3, n_2 equal to 2 and channel number C is 1.

$$\text{derive from eq. (24)} \begin{cases} \frac{\partial \ell}{\partial b_1^2} = (p_{11} - y_{11}) + (p_{21} - y_{21}) \\ \frac{\partial \ell}{\partial b_2^2} = (p_{12} - y_{12}) + (p_{22} - y_{22}) \end{cases} \quad (28)$$

$$\text{derive from eq. (25)} \left\{ \begin{array}{ll} \frac{\partial \ell}{\partial w_{11}^2} &= (p_{11} - y_{11})\sigma_{11} + (p_{21} - y_{21})\sigma_{12} \\ \frac{\partial \ell}{\partial w_{12}^2} &= (p_{11} - y_{11})\sigma_{21} + (p_{21} - y_{21})\sigma_{22} \\ &\dots \\ \frac{\partial \ell}{\partial w_{n_1}^2} &= (p_{11} - y_{11})\sigma_{n_1 1} + (p_{21} - y_{21})\sigma_{n_1 2} \\ \frac{\partial \ell}{\partial w_{21}^2} &= (p_{12} - y_{12})\sigma_{11} + (p_{22} - y_{22})\sigma_{12} \\ \frac{\partial \ell}{\partial w_{22}^2} &= (p_{12} - y_{12})\sigma_{21} + (p_{22} - y_{22})\sigma_{22} \\ &\dots \\ \frac{\partial \ell}{\partial w_{n_1}^2} &= (p_{12} - y_{12})\sigma_{n_1 1} + (p_{22} - y_{22})\sigma_{n_1 2} \end{array} \right. \quad (29)$$

$$\text{derive from eq. (26)} \left\{ \begin{array}{ll} \frac{\partial \ell}{\partial b_{\underline{1}}^1} &= \sum_{i=1}^{(d')^2} w_{1i}^2 [(p_{11} - y_{11})\sigma'_{i1} + (p_{21} - y_{21})\sigma'_{i2}] + \\ &\quad \sum_{i=1}^{(d')^2} w_{2i}^2 [(p_{12} - y_{12})\sigma'_{i1} + (p_{22} - y_{22})\sigma'_{i2}] \\ \frac{\partial \ell}{\partial b_{\underline{2}}^1} &= \sum_{i=(d')^2+1}^{2*(d')^2} w_{1i}^2 [(p_{11} - y_{11})\sigma'_{i1} + (p_{21} - y_{21})\sigma'_{i2}] + \\ &\quad \sum_{i=(d')^2+1}^{2*(d')^2} w_{2i}^2 [(p_{12} - y_{12})\sigma'_{i1} + (p_{22} - y_{22})\sigma'_{i2}] \\ \frac{\partial \ell}{\partial b_{\underline{3}}^1} &= (\sum_{i=2*(d')^2+1}^{3*(d')^2} w_{1i}^2 [(p_{11} - y_{11})\sigma'_{i1} + (p_{21} - y_{21})\sigma'_{i2}] + \\ &\quad \sum_{i=2*(d')^2+1}^{3*(d')^2} w_{2i}^2 [(p_{12} - y_{12})\sigma'_{i1} + (p_{22} - y_{22})\sigma'_{i2}]) \end{array} \right. \quad (30)$$

$$\text{derive from eq. (26)} \left\{ \begin{array}{ll} \frac{\partial \ell}{\partial b_{\underline{1}}^1} &= \sum_{i=1}^{d'} \sum_{j=1}^{d'} \frac{\partial \ell}{\partial z_{1ij}} = \sum_{i=1}^{(d')^2} \frac{\partial \ell}{\partial H[r_i]} = \sum_{j=1}^{n_2} (p_{.j} - y_{.j}) \sum_{i=1}^{(d')^2} w_{jr_i}^2 \sigma'_{r_i} \\ &\dots \\ \frac{\partial \ell}{\partial b_{\underline{2}}^1} &= \sum_{i=1}^{d'} \sum_{j=1}^{d'} \frac{\partial \ell}{\partial z_{2ij}} = \sum_{i=1}^{(d')^2} \frac{\partial \ell}{\partial H[r_i]} = \sum_{j=1}^{n_2} (p_{.j} - y_{.j}) \sum_{i=1}^{(d')^2} w_{jr_i}^2 \sigma'_{r_i} \end{array} \right. \quad (31)$$

$$\text{derive from eq. (27)} \left\{ \begin{array}{ll} \frac{\partial E}{\partial w_{1gh}^1} &= \sum_{m=1}^{(d')^2} w_{1m}^2 [(p_{11} - y_{11})\sigma'_{m1} \sum_{i=1}^{d'} \sum_{j=1}^{d'} \hat{x}_{1,si+g-1,sj+h-1} \\ &\quad + (p_{21} - y_{21})\sigma'_{m2} \sum_{i=1}^{d'} \sum_{j=1}^{d'} \hat{x}_{2,si+g-1,sj+h-1}] \\ &\quad + \sum_{m=1}^{(d')^2} w_{2m}^2 [(p_{12} - y_{12})\sigma'_{m1} \sum_{i=1}^{d'} \sum_{j=1}^{d'} \hat{x}_{1,si+g-1,sj+h-1} \\ &\quad + (p_{22} - y_{22})\sigma'_{m2} \sum_{i=1}^{d'} \sum_{j=1}^{d'} \hat{x}_{2,si+g-1,sj+h-1}] \\ \frac{\partial E}{\partial w_{2gh}^1} &= \sum_{m=(d')^2+1}^{2*(d')^2} w_{1m}^2 [(p_{11} - y_{11})\sigma'_{m1} \sum_{i=1}^{d'} \sum_{j=1}^{d'} \hat{x}_{1,si+g-1,sj+h-1} \\ &\quad + (p_{21} - y_{21})\sigma'_{m2} \sum_{i=1}^{d'} \sum_{j=1}^{d'} \hat{x}_{2,si+g-1,sj+h-1}] \\ &\quad + \sum_{m=(d')^2+1}^{2*(d')^2} w_{2m}^2 [(p_{12} - y_{12})\sigma'_{m1} \sum_{i=1}^{d'} \sum_{j=1}^{d'} \hat{x}_{1,si+g-1,sj+h-1} \\ &\quad + (p_{22} - y_{22})\sigma'_{m2} \sum_{i=1}^{d'} \sum_{j=1}^{d'} \hat{x}_{2,si+g-1,sj+h-1}] \\ \frac{\partial E}{\partial w_{3gh}^1} &= \sum_{m=2*(d')^2+1}^{3*(d')^2} w_{1m}^2 [(p_{11} - y_{11})\sigma'_{m1} \sum_{i=1}^{d'} \sum_{j=1}^{d'} \hat{x}_{1,si+g-1,sj+h-1} \\ &\quad + (p_{21} - y_{21})\sigma'_{m2} \sum_{i=1}^{d'} \sum_{j=1}^{d'} \hat{x}_{2,si+g-1,sj+h-1}] \\ &\quad + \sum_{m=2*(d')^2+1}^{3*(d')^2} w_{2m}^2 [(p_{12} - y_{12})\sigma'_{m1} \sum_{i=1}^{d'} \sum_{j=1}^{d'} \hat{x}_{1,si+g-1,sj+h-1} \\ &\quad + (p_{22} - y_{22})\sigma'_{m2} \sum_{i=1}^{d'} \sum_{j=1}^{d'} \hat{x}_{2,si+g-1,sj+h-1}] \end{array} \right. \quad (32)$$

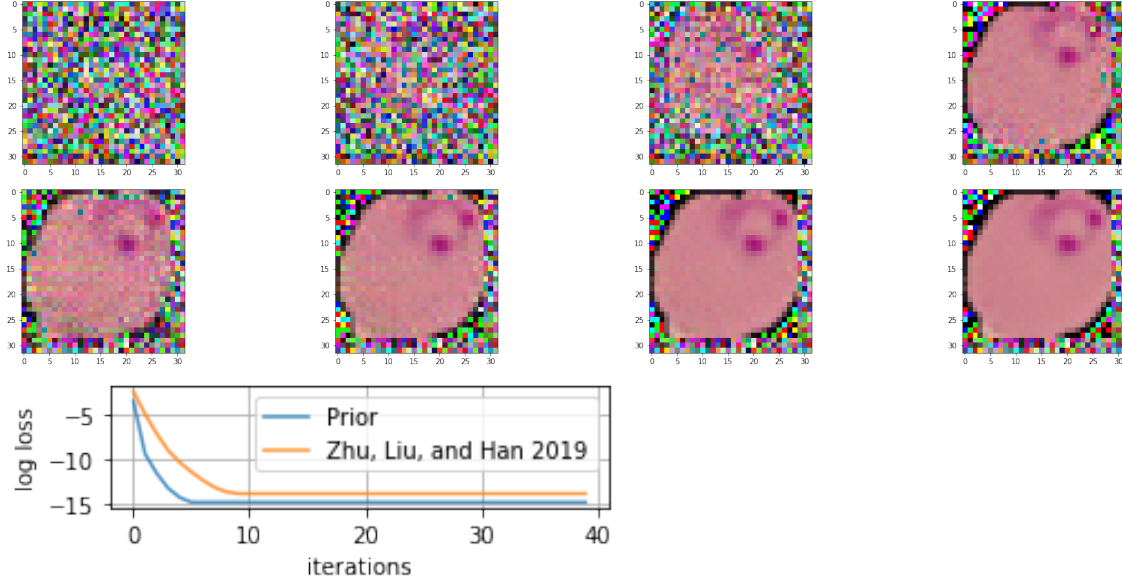


Figure 13: *CELL*: The first row corresponds to the reconstruction by [1], for 10, 20, 30, and final iteration, whereas the second row is produced by our method.

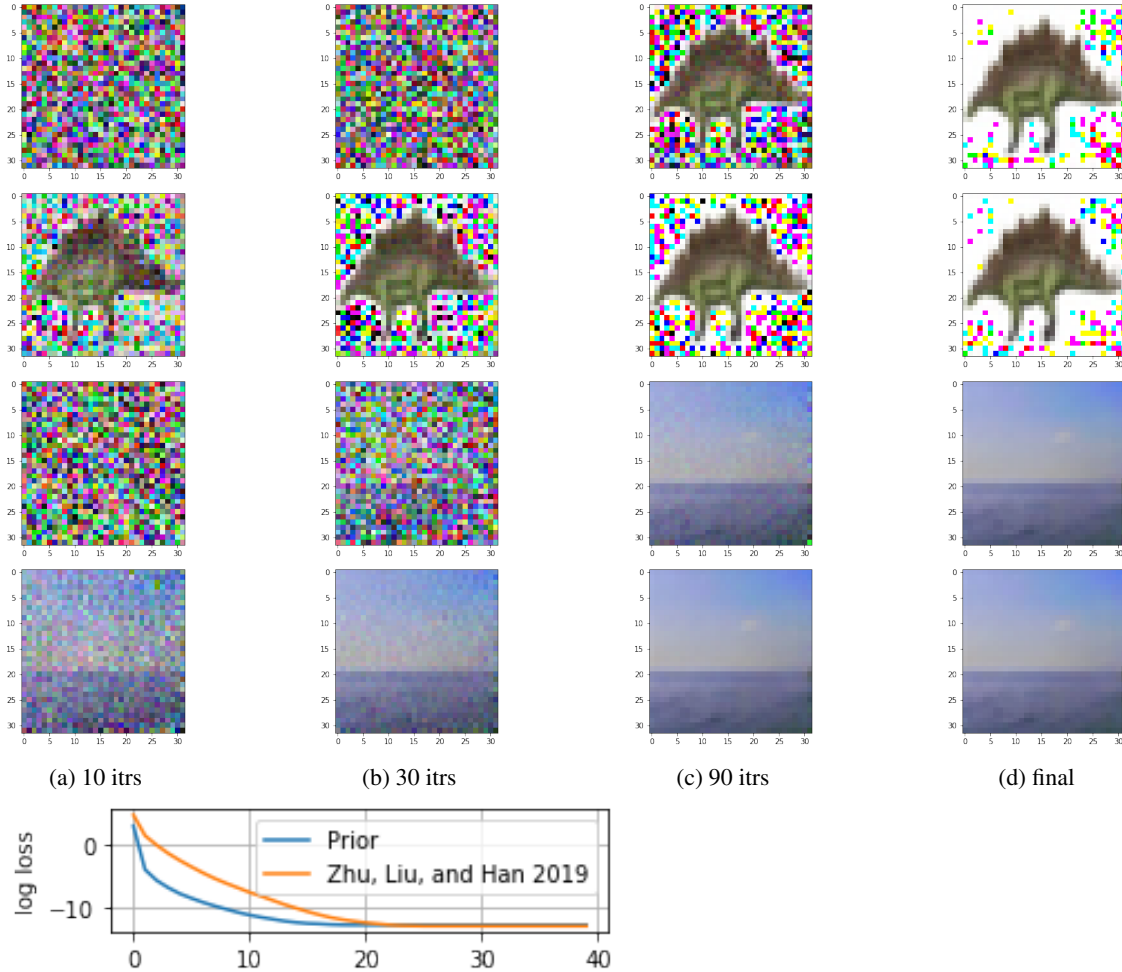


Figure 14: *Cifar100*: We show partial reconstruction for 10 (col.1), 30 (col.2), 90 (col.3) and final (col.4) iteration. The odd number of rows (1,3) are produced by [1] and even number of rows (2,4) are produced by our method. The corresponding log-scale loss is shown under the reconstruction procedure.

References

- [1] Ligeng Zhu, Zhijian Liu, and Song Han. Deep leakage from gradients. In *Advances in Neural Information Processing Systems*, pages 14774–14784, 2019.
- [2] Jakub Konečný, H Brendan McMahan, Felix X Yu, Peter Richtárik, Ananda Theertha Suresh, and Dave Bacon. Federated learning: Strategies for improving communication efficiency. *arXiv preprint arXiv:1610.05492*, 2016.
- [3] Peter Kairouz, H Brendan McMahan, Brendan Avent, Aurélien Bellet, Mehdi Bennis, Arjun Nitin Bhagoji, Keith Bonawitz, Zachary Charles, Graham Cormode, Rachel Cummings, et al. Advances and open problems in federated learning. *arXiv preprint arXiv:1912.04977*, 2019.
- [4] Cynthia Dwork. Differential privacy: A survey of results. In *International conference on theory and applications of models of computation*, pages 1–19. Springer, 2008.
- [5] Arjun Nitin Bhagoji, Supriyo Chakraborty, Prateek Mittal, and Seraphin Calo. Analyzing federated learning through an adversarial lens. In *International Conference on Machine Learning*, pages 634–643, 2019.
- [6] Ziteng Sun, Peter Kairouz, Ananda Theertha Suresh, and H Brendan McMahan. Can you really backdoor federated learning? *arXiv preprint arXiv:1911.07963*, 2019.
- [7] Briland Hitaj, Giuseppe Ateniese, and Fernando Perez-Cruz. Deep models under the gan: information leakage from collaborative deep learning. In *Proceedings of the 2017 ACM SIGSAC Conference on Computer and Communications Security*, pages 603–618, 2017.
- [8] Zhibo Wang, Mengkai Song, Zhifei Zhang, Yang Song, Qian Wang, and Hairong Qi. Beyond inferring class representatives: User-level privacy leakage from federated learning. In *IEEE INFOCOM 2019-IEEE Conference on Computer Communications*, pages 2512–2520. IEEE, 2019.
- [9] Luca Melis, Congzheng Song, Emiliano De Cristofaro, and Vitaly Shmatikov. Exploiting unintended feature leakage in collaborative learning. In *2019 IEEE Symposium on Security and Privacy (SP)*, pages 691–706. IEEE, 2019.
- [10] Matthew Fredrikson, Eric Lantz, Somesh Jha, Simon Lin, David Page, and Thomas Ristenpart. Privacy in pharmacogenetics: An end-to-end case study of personalized warfarin dosing. In *23rd {USENIX} Security Symposium ({USENIX} Security 14)*, pages 17–32, 2014.
- [11] Bo Zhao, Konda Reddy Mopuri, and Hakan Bilen. idlg: Improved deep leakage from gradients. *arXiv preprint arXiv:2001.02610*, 2020.
- [12] Jonas Geiping, Hartmut Bauermeister, Hannah Dröge, and Michael Moeller. Inverting gradients—how easy is it to break privacy in federated learning? *arXiv preprint arXiv:2003.14053*, 2020.
- [13] Yann N Dauphin, Razvan Pascanu, Caglar Gulcehre, Kyunghyun Cho, Surya Ganguli, and Yoshua Bengio. Identifying and attacking the saddle point problem in high-dimensional non-convex optimization. In *Advances in neural information processing systems*, pages 2933–2941, 2014.
- [14] Ian Goodfellow, Yoshua Bengio, Aaron Courville, and Yoshua Bengio. *Deep learning*, volume 1. MIT Press, 2016.